CHEST

Original Research

INTERVENTIONAL PULMONOLOGY

Volumetric Optical Frequency Domain Imaging of Pulmonary Pathology With Precise Correlation to Histopathology

Lida P. Hariri, MD, PhD; Matthew B. Applegate, BS; Mari Mino-Kenudson, MD; Eugene J. Mark, MD; Benjamin D. Medoff, MD; Andrew D. Luster, MD, PhD; Brett E. Bouma, PhD; Guillermo J. Tearney, MD, PhD; and Melissa J. Suter, PhD

Background: **Lung cancer is the leading cause of cancer-related mortality. Radiology and bronchoscopy techniques do not have the necessary resolution to evaluate lung lesions on the microscopic scale, which is critical for diagnosis. Bronchial biopsy specimens can be limited by sampling error and small size. Optical frequency domain imaging (OFDI) provides volumetric views of tissue microstructure at near-histologic resolution and may be useful for evaluating pulmonary lesions to increase diagnostic accuracy. Bronchoscopic OFDI has been evaluated in vivo, but a lack of correlated histopathology has limited the ability to develop accurate image interpretation criteria.**
Methods: **We performed OFDI through two approaches (airway-centered and parenchymal imaging) in 22 ex vivo lung specimens, using tissue dye to precisely correlate imaging and histology.**
Results: **OFDI of normal airway allowed visualization of epithelium, lamina propria, cartilage, and alveolar attachments. Carcinomas exhibited architectural disarray, loss of normal airway and alveolar structure, and rapid light attenuation. Squamous cell carcinomas showed nested architecture. Atypical glandular formation was appreciated in adenocarcinomas, and uniform trabecular gland formation was seen in salivary gland carcinomas. Mucinous adenocarcinomas showed alveolar wall thickening with intraalveolar mucin. Interstitial fibrosis was visualized as signal-dense tissue, with an interstitial distribution in mild interstitial fibrotic disease and a diffuse subpleural pattern with cystic space formation in usual interstitial pneumonitis.**
Conclusions: **To our knowledge, this study is the first demonstration of volumetric OFDI with precise correlation to histopathology in lung pathology. We anticipate that OFDI may play a role in assessing airway and parenchymal pathology, providing fresh insights into the volumetric features of pulmonary disease.**
CHEST 2013; 143(1):64–74

Abbreviations: OCT = optical coherence tomography; OFDI = optical frequency domain imaging; SCC = squamous cell carcinoma; UIP = usual interstitial pneumonitis

Lung cancer is the leading cause of cancer-related deaths.[1] Early identification of lung malignancy can be limited by radiologic resolution and the inability to visualize microscopic changes and tissue beyond the airway surface during bronchoscopy. Lung biopsy and fine needle aspiration specimens can be limited by the small amounts of tissue obtained and sampling error. Larger tissue volumes can improve diagnostic yield but require significantly more invasive procedures, such as video-assisted thoracoscopic wedge resection, to obtain additional tissue. The ability to visualize larger tissue volumes by imaging techniques with high resolution during bronchoscopy or CT scan-guided percutaneous procedures could potentially confirm biopsy site selection of targeted lesions and provide considerably more architectural information that may be used to aid diagnosis without necessitating a more invasive procedure.

Optical coherence tomography (OCT) is a noninvasive, noncontact, optical imaging modality that generates high-resolution cross-sectional images of tissue

For editorial comment see page 10

microstructure with penetration depths approaching 2 to 3 mm.[2,3] The high resolution (< 10 μm) is comparable to that of low-power ($\times 4$) bright-field microscopy, which is sufficient for detecting microscopic

tissue architecture. Optical frequency domain imaging (OFDI), also called swept source OCT or frequency domain OCT, is a second-generation OCT imaging technology with the capability to image at more rapid acquisition rates (100-fold increase).[4-8] The rapid acquisition rates provided by OFDI allow for large-area volumetric, high-resolution imaging, which is ideal for evaluating long segments of the tracheobronchial tree during bronchoscopy. OCT and OFDI are nondestructive imaging techniques and have been used in a variety of applications to assess pathology, including catheter-based cardiovascular[5,9-17] and GI[3,5,18-23] applications, with high accuracy.

OCT has been used to evaluate pulmonary airways[24,25] and parenchyma[26,27] in animal models and in vivo in human airway,[28,29] demonstrating the ability to delineate airway layering and alveolar attachments. OCT evaluation of bronchial lesions in vivo during bronchoscopy has been useful in characterizing preinvasive lesions of the bronchial mucosa.[30-33] Volumetric optical imaging has been conducted to assess bronchial lumen dimensions with anatomic OCT, a long-image ranging depth OCT hybrid.[34-42] The feasibility of OFDI to image bronchial mucosa was recently demonstrated in a short segment of bronchus (0.8 cm),[43] and volumetric OFDI spanning multiple airway generations in swine and human pulmonary airways in vivo has recently been reported.[44]

Although OCT and OFDI imaging of pulmonary pathology in vivo has demonstrated capabilities to visualize pathologic changes, identification of imaging features has not been performed to date because of difficulties in obtaining precisely correlated tissue. Without adequate correlation to histopathology, imaging features of pulmonary pathology cannot be ascertained, and interpretation of in vivo bronchoscopic and percutaneous OFDI images is hindered. Precisely matched tissue is essential to provide gold standard correlates required to accurately assess imaging features. However, even if biopsy sites were accurately correlated with OCT/OFDI in vivo, the biopsy specimens obtained during bronchoscopy and other in vivo procedures often are small and superficial and are thus insufficient to provide a correlate for image feature assessment. To appropriately characterize OFDI or OCT imaging features of both normal and pathologic bronchial airway and lung parenchyma, images need to be correlated on a one-to-one basis with larger portions of tissue for histopathology, which can only be performed in the ex vivo setting. In this study, we perform volumetric OFDI through two approaches—bronchoscopic airway-centered imaging and parenchymal imaging—on surgical and autopsy lung specimens and directly correlate imaging features with one-to-one matched histopathology.

Materials and Methods

Imaging System and Catheters

The technical details of OFDI have been described previously.[5,6] Images were obtained at 10 to 50 frames/s with either custom-built bronchoscopic 2.4F to 5.1F (0.8-1.7 mm diameter) helical scanning catheters or a dual-axis benchtop scanner. The axial resolution of the OFDI system was 6 μm in tissue.[5,7]

Image Acquisition

The Partners Human Research Committee Institutional Review Board approved this study (protocol number 2010-P-002214/1). We performed OFDI on fresh, uninflated surgical resection and autopsy lung specimens prior to fixation through two approaches: bronchoscopic airway-centered imaging and parenchymal imaging. The airway or parenchyma containing the tissue region of interest was bisected, and two marks were placed approximately 1 to 2 cm apart to define the OFDI/histopathology imaging window. The registration marks were created using 24-gauge needle pins and tissue dye (Triangle Biomedical Sciences). OFDI imaging was then conducted, encompassing the imaging window and registration marks to allow for exact correlation with histopathology. The tissue samples were subsequently fixed in formalin and submitted for histologic processing. Tissue samples were oriented and embedded in paraffin to ensure that the resulting sections contained both registration marks for correlation with OFDI images. OFDI and histologic images were registered based on the location of the inked needle marks, which were about 100 μm in diameter. The details of the ink mark registration procedure have been previously described in detail.[45] To provide an assessment of a true normal, healthy human airway and alveolar attachments, in vivo OFDI imaging was also performed bronchoscopically in a healthy 27-year-old female volunteer (Fig 1).

Image Processing and Interpretation

The OFDI images were generated from the raw data sets off line. Frame averaging (two to five frames) was performed to reduce the speckle noise observed within the OFDI images shown in Figures 2 through 7.[46] Image filtering and longitudinal and three-dimensional representations were prepared using ImageJ 1.38w

Manuscript received November 2, 2011; revision accepted February 13, 2012.
Affiliations: From the Department of Pathology (Drs Hariri, Mino-Kenudson, Mark, and Tearney); Pulmonary and Critical Care Unit (Mr Applegate and Drs Medoff and Suter); Wellman Center for Photomedicine (Drs Hariri, Bouma, Tearney, and Suter and Mr Applegate); and Rheumatology, Allergy and Immunology Division (Dr Luster), Massachusetts General Hospital, Boston; Harvard Medical School (Drs Hariri, Mino-Kenudson, Mark, Medoff, Luster, Bouma, Tearney, and Suter), Cambridge; and Harvard-MIT Division of Health Sciences and Technology (Drs Bouma and Tearney), Cambridge, MA.
Funding/Support: This work was funded in part by the National Institutes of Health [Grants R00CA134920, R37AI040618, U19AI095261, P41EB01590] and the American Lung Association [Grant RG-194681-N].
Correspondence to: Melissa J. Suter, PhD, Massachusetts General Hospital, 55 Fruit St, Warren Bldg, Room 408D, Boston, MA 02114; e-mail: msuter@partners.org
© 2013 American College of Chest Physicians. Reproduction of this article is prohibited without written permission from the American College of Chest Physicians. See online for more details.
DOI: 10.1378/chest.11-2797

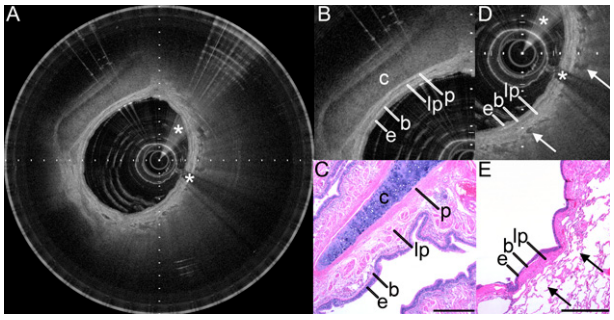

FIGURE 1. In vivo bronchoscopic catheter-based optical frequency domain imaging (OFDI) of a normal airway. A, OFDI cross-section of airway. B, Higher magnification view of airway cross-section visualizing typical layering of airway, including respiratory epithelium (e), transition between epithelium and underlying basement membrane/lamina propria (b), lamina propria (lp), perichondrium (p), and cartilage (c). C, Representative histology from a normal airway demonstrating similar layering to the in vivo OFDI airway image in B (hematoxylin and eosin stain). D, Higher magnification view of airway cross-section with attached alveolar attachments (arrows), with overlying respiratory epithelium (e), transition between epithelium and underlying basement membrane/lamina propria (b), and lamina propria (lp). E, Representative histology from a normal airway demonstrating similar layering and alveolar attachments as seen in the in vivo OFDI airway image in D (hematoxylin and eosin stain). OFDI imaging artifacts are denoted by asterisks. Tick marks in OFDI images are 0.5 mm. Scale bars on histology images are 0.5 mm.

(National Institutes of Health) and Osirix 2.75 (University Hospital of Geneva) software, respectively. Images are displayed by use of a grayscale lookup table.

Pathologic Interpretation of OFDI Data

A team of pathologists and OFDI experts interpreted the OFDI images and reached a consensus off-line. Interpretation was based on architectural morphology seen in both the OFDI and the correlated histopathology.

RESULTS

OFDI was performed in 22 lung specimens (20 surgical and two autopsy) as follows: 12 adenocarcinomas, four squamous cell carcinomas (SCCs), one tracheal adenoid cystic carcinoma, one cartilaginous hamartoma, and four interstitial fibrosis cases. In these specimens, an additional 16 regions of normal lung were evaluated with matched OFDI and histopathology. A summary of the imaging findings are presented in Table 1. Following, we describe representative cases from the corresponding OFDI-histology data set. There were no features observed in the OFDI images that were not visualized in the histopathology slides. As expected, because of the increased resolution of high-power microscopy, not all of the finer features observed in the histology slides were visible in the OFDI images. The size of features observed in the OFDI and histology images correlated well, which is demonstrated in the figures by the location of the ink marks in OFDI and histology (indicated with asterisks) as well as by the scale bars. In some cases, however, we observed minor shrinkage (<5%) of the histology tissue, which is a well-known histopathology processing artifact due to the tissue fixation process.[47] All OFDI imaging features described in this section (Table 1) were applicable to all specimens of the respective pathology category. Features that were not consistently found in all samples of a specific pathology category were omitted.

Normal Lung

In OFDI of normal in vivo airway shown in Figure 1, the respiratory epithelium (e) is visible as a thin layer at the luminal aspect of the airway, with homogeneous,

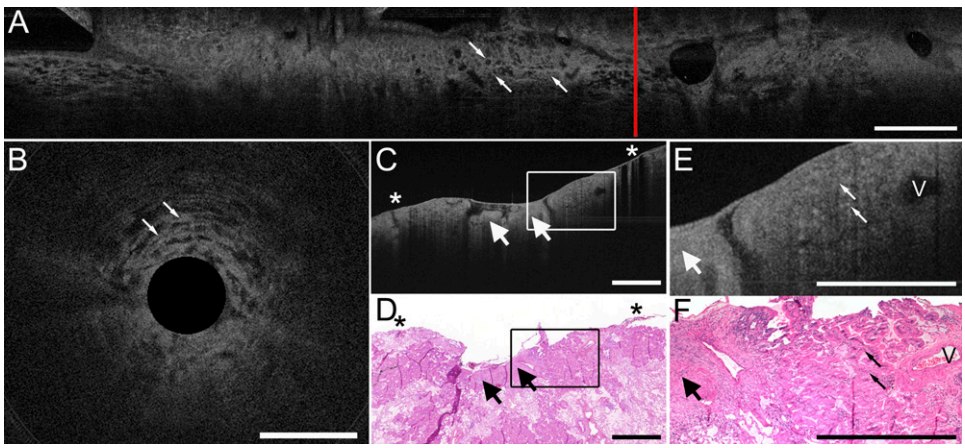

FIGURE 2. Parenchymal OFDI of mucinous adenocarcinoma. A, OFDI catheter-based longitudinal section (scale bar = 5.0 mm). B, OFDI catheter-based cross section at site of red line on A (scale bar = 1.0 mm). C and D, OFDI benchtop longitudinal section (C) and corresponding histology (D) (hematoxylin and eosin stain, scale bars = 1.0 mm). E and F, Higher magnification of OFDI benchtop longitudinal section from C and D (E) and corresponding histology at location of box in C and D (hematoxylin and eosin stain, scale bar = 1.0 mm). Narrow arrows indicate thickened, signal-intense alveolar walls, and wide arrows indicate tumor-associated scar. Ink marks are denoted by the asterisks. V denotes blood vessel. See Figure 1 legend for expansion of abbreviation.

moderate signal intensity. There is an underlying thin, signal-intense band (b) consistent with the transition from epithelium to the underlying connective tissue of the basement membrane and lamina propria (lp). The lamina propria consists of organized signal-intense to signal-poor tissue, corresponding to the various components of the lamina propria, such as signal-intense connective tissue and signal-poor peribronchial glandular tissue. The smooth muscle surrounding the bronchial mucosa is dispersed among the loose stroma of the lamina propria and does not form a distinct layer; thus, a definitive muscularis mucosa cannot be identified as is seen in other tubular organs, such as the GI tract. Cartilage (c) appears as homogeneous, signal-poor crescentic structures with well-delineated boundaries. The perichondrium (p) appears as a thin layer of signal-intense tissue encompassing the cartilage. Alveolar attachments (arrows) are visible as thin, signal-intense lattice-like alveolar walls with signal-void alveolar spaces.

Neoplastic Pulmonary Pathology

Mucinous Adenocarcinoma: In pleural-based OFDI, mucinous adenocarcinoma (Fig 2) appears as a mass with ill-defined boundaries and heterogeneous, mildly increased signal attenuation. Within the mass, the lattice-like architecture of the alveoli is preserved but displays alveolar wall thickening with increased signal intensity when compared with the normal alveolar structures (Fig 1). The signal-intense alveolar wall thickening corresponds to mucinous epithelial tumor

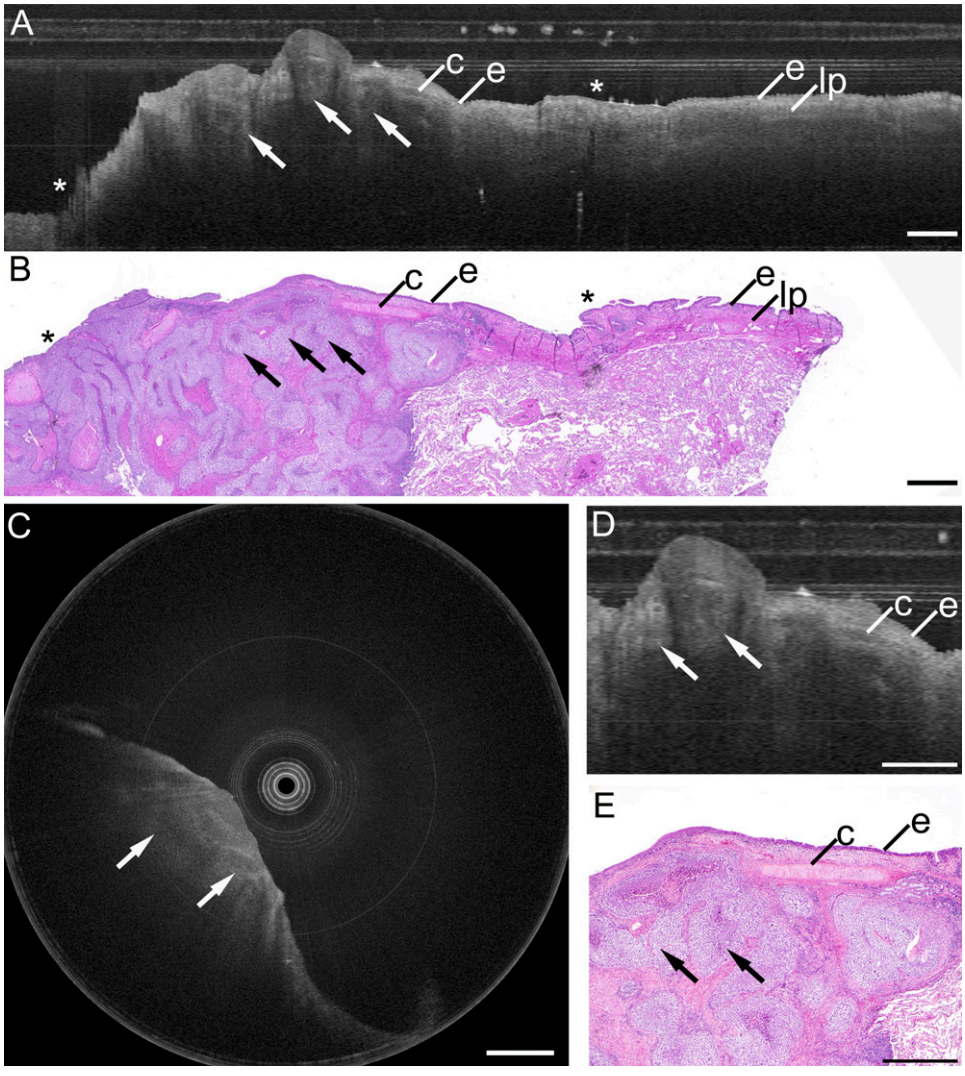

FIGURE 3. Bronchoscopic catheter-based OFDI of squamous cell carcinoma, basaloid type. A, OFDI longitudinal section. B, Corresponding histology (hematoxylin and eosin stain). C, OFDI cross-section. D and E, Higher magnification OFDI longitudinal section (D) and corresponding histology (E), showing epithelium (e), lamina propria (lp), and cartilage (c) (hematoxylin and eosin stain). Arrows indicate nests of hyperintense squamous cell carcinoma with signal-poor central necrosis. Ink marks are denoted by asterisks. Scale bars = 1.0 mm. See Figure 1 legend for expansion of abbreviation.

cells lining the alveolar spaces (narrow arrows). Focal accumulations of signal-poor, amorphous material within the alveolar spaces are appreciated, consistent with intraalveolar mucin. There is also a region of homogenous, signal-intense, rapidly attenuating tissue in the center of the mass, which corresponds histologically to a tumor-associated scar (wide arrows). Blood vessels (V) within the mass can also be visualized.

SCC, Basaloid Type: OFDI imaging of SCC, basaloid type, through the airway (Fig 3) reveals a loss of the typical layered architecture observed in the normal airway (Fig 1), which is disrupted by an ill-defined, mass-forming lesion with rapid, heterogeneous signal attenuation. The tumor consists of ill-defined nodules with a high signal-intense periphery and central signal-poor to signal-void regions, which correlate with nests of malignant squamous cells with central necrosis, respectively (arrows). On the right side of the image shown in Figure 3, some residual normal airway architecture can be appreciated, including respiratory epithelium (e), lamina propria (lp), and a portion of cartilage (c), which are present in corresponding histopathology. No gland formation is appreciated.

Adenoid Cystic Carcinoma: OFDI of adenoid cystic carcinoma (Fig 4) reveals an endobronchial mass with luminal obstruction. Uniform, signal-intense trabeculation and small gland formation typical of adenoid cystic carcinomas can be appreciated in OFDI (wide arrows) and is confirmed in the corresponding histopathology. Microcystic lumen formation is evident in OFDI (narrow arrows) as small, signal-void regions with well-defined borders within the mass, with mucin filled lumens appearing as small, signal-poor regions with well-defined borders. However, the presence of such microcystic spaces is variable in adenoid cystic carcinomas. Respiratory epithelium (e) overlying the mass is visible in OFDI and histopathology and may be present in these types of lesions. On the aspect of the bronchus opposite the mass shown in Figure 4, normal layered airway architecture can be appreciated, including respiratory epithelium (e), lamina propria (lp), and cartilage (c), which are present in corresponding histopathology and similar to the airway layering seen in the normal in vivo bronchus (Fig 1). Mild thickening of the lamina propria is visible in OFDI with homogeneously increased signal intensity, which correlates to mild fibrosis of the lamina propria in the corresponding histopathology.

Benign Pulmonary Pathology

Cartilaginous Hamartoma: OFDI imaging of cartilaginous hamartoma (Fig 5) reveals a lobulated mass with well-delineated borders. Evenly dispersed, fine-scale regions of high signal intensity appear in a background of uniform, moderate signal intensity. The signal intensity of cartilaginous hamartoma appears more intense than encountered in normal cartilage of

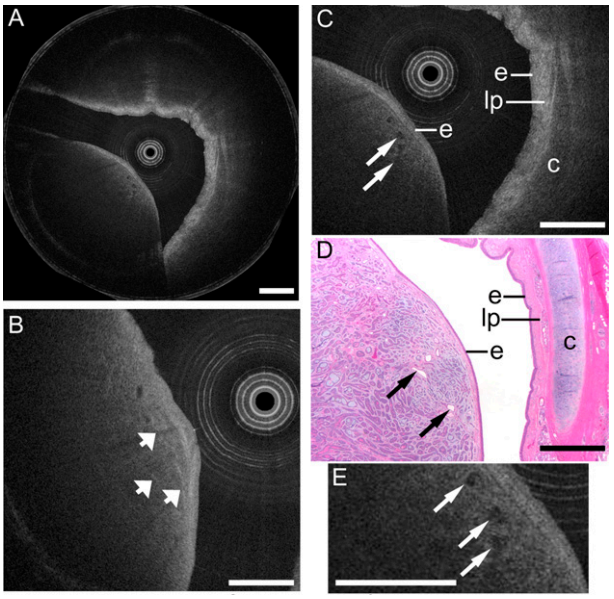

FIGURE 4. Bronchoscopic catheter-based OFDI of adenoid cystic carcinoma. A, OFDI cross section. B, OFDI cross section with trabecular structures (wide arrows). C and D, OFDI cross section (C) and corresponding histology (D), showing epithelium (e), lamina propria with mild fibrosis (lp), and cartilage (c) (hematoxylin and eosin stain). E, Higher magnification of OFDI cross section. Wide arrows indicate uniform trabecular and glandular structures. Narrow arrows indicate small microcystic spaces filled with mucin. Scale bars = 1.0 mm. See Figure 1 legend for expansion of abbreviation.

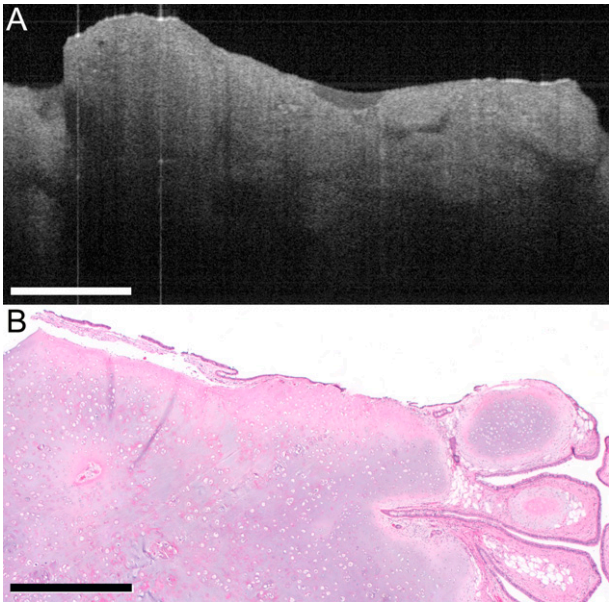

FIGURE 5. Parenchymal benchtop OFDI of cartilaginous hamartoma. A, OFDI longitudinal section. B, Corresponding histopathology (hematoxylin and eosin stain). OFDI reveals a lobulated mass with well-defined boundaries and evenly dispersed, fine-scale regions of high signal intensity in a background of uniform, moderate signal intensity. Scale bars = 1.0 mm.

bronchial cartilaginous rings. The three-dimensional rendering of the hamartoma accentuates the lobulated architecture and homogeneity of imaging features throughout the mass (Video 1).

Interstitial Fibrosis

Idiopathic Interstitial Fibrosis-Usual Interstitial Pneumonitis: OFDI imaging in the presented case of usual interstitial pneumonitis (UIP) (Fig 6) was performed by imaging through the pleural surface as opposed to imaging through cut pleura. Imaging reveals characteristic dense subpleural fibrosis seen as disorganized signal-dense tissue (F) underlying the pleura (P). There are appreciable, irregularly shaped cystic, signal-void to signal-poor spaces with variably defined borders, which correspond to subpleural honeycomb change on histopathology (boxes). Mucin-filled honeycomb spaces appear to be signal poor, whereas honeycomb spaces lacking mucin appear to be signal void. In this case of UIP, the disease was advanced with more diffuse fibrosis than is typically seen in classic UIP; thus, only very minimal areas of uninvolved lung were present on further histopathologic evaluation. No regions of normal-appearing lung parenchyma are seen in the locations of the specimen imaged with OFDI.

Mild Pleural and Subpleural Interstitial Fibrosis: Mild, focal pleural and subpleural interstitial fibrosis are common incidental findings, especially in areas with prior inflammation. In the presented case of mild pleural and subpleural interstitial fibrosis imaged with OFDI through the pleural surface (Fig 7), the pleura (P) is focally thickened with signal-dense tissue (F). There are intervening signal-void spaces (arrows) with mildly thickened, lattice-like alveolar walls compared with normal alveoli visualized in vivo (Fig 1). Comparison with corresponding histopathology reveals focal pleural and subpleural fibrosis with admixed alveoli, some of which show mild interstitial thickening. Compared with the case of UIP (Fig 6), the fibrosis in both cases has similar imaging features with respect to signal intensity. However, the case of UIP shows more diffuse subpleural fibrosis with subpleural cystic spaces, which are larger in diameter than the alveoli seen in the case of mild pleural and subpleural interstitial fibrosis.

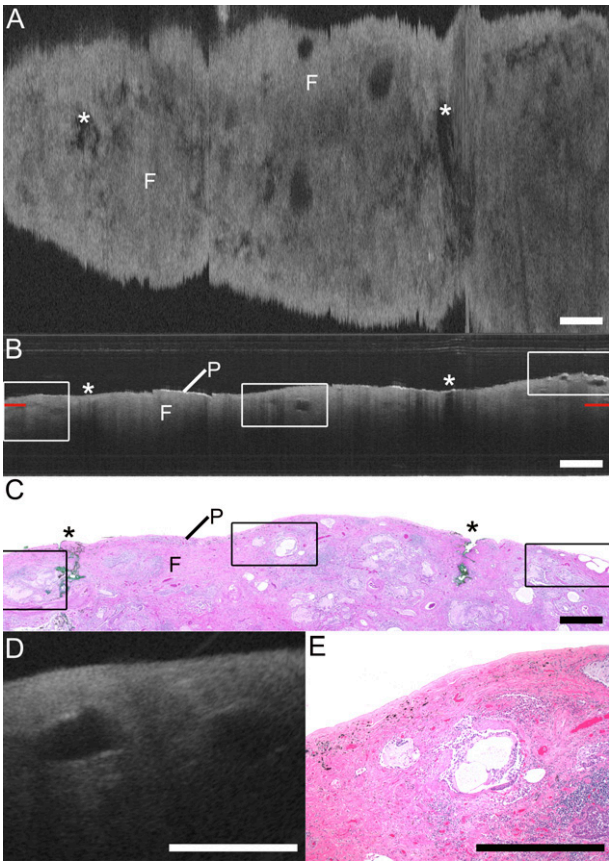

FIGURE 6. Pleural catheter-based OFDI of usual interstitial pneumonitis showing the pleural surface (P) and subpleural fibrosis (F). A, En face OFDI at location of red side tick marks in B. B and C, OFDI longitudinal section (B) and corresponding histopathology (C) (hematoxylin and eosin stain). D, OFDI cross section. E, Histopathology from the longitudinal section corresponding to subpleural cyst in D (hematoxylin and eosin stain). Boxed regions indicated subpleural cystic spaces, and ink marks are denoted by asterisks. Scale bars = 1.0 mm. See Figure 1 legend for expansion of abbreviation.

DISCUSSION

To our knowledge, this study is the first demonstration of volumetric high-resolution OFDI with precise correlation to tissue-based diagnostics for evaluating lung tumors and other lung pathology. Prior work using OCT and OFDI for in vivo lung imaging have demonstrated safety, feasibility, the ability to visualize normal airway layering and alveolar attachments and the potential to identify pathologic changes.[24-44] However, specific imaging features of airway and parenchymal pathology seen with OCT or OFDI could not be confirmed by histopathology because of difficulties in registration and the small biopsy specimen size obtained during in vivo procedures. Before OCT or OFDI can play any significant role in the assessment of pulmonary disease in vivo, it is critical that specific imaging criteria be developed and validated. This requires direct correlation between imaging and histopathology that cannot be performed in vivo. In this study of ex vivo pulmonary airway and parenchymal OFDI, the one-to-one correlation obtained between OFDI and histopathology allows for the identification of fine imaging features for pulmonary malignancies, benign lesions, and interstitial fibrosis.

Bronchoscopic OFDI has the potential to identify the optimal biopsy site during standard bronchoscopy,

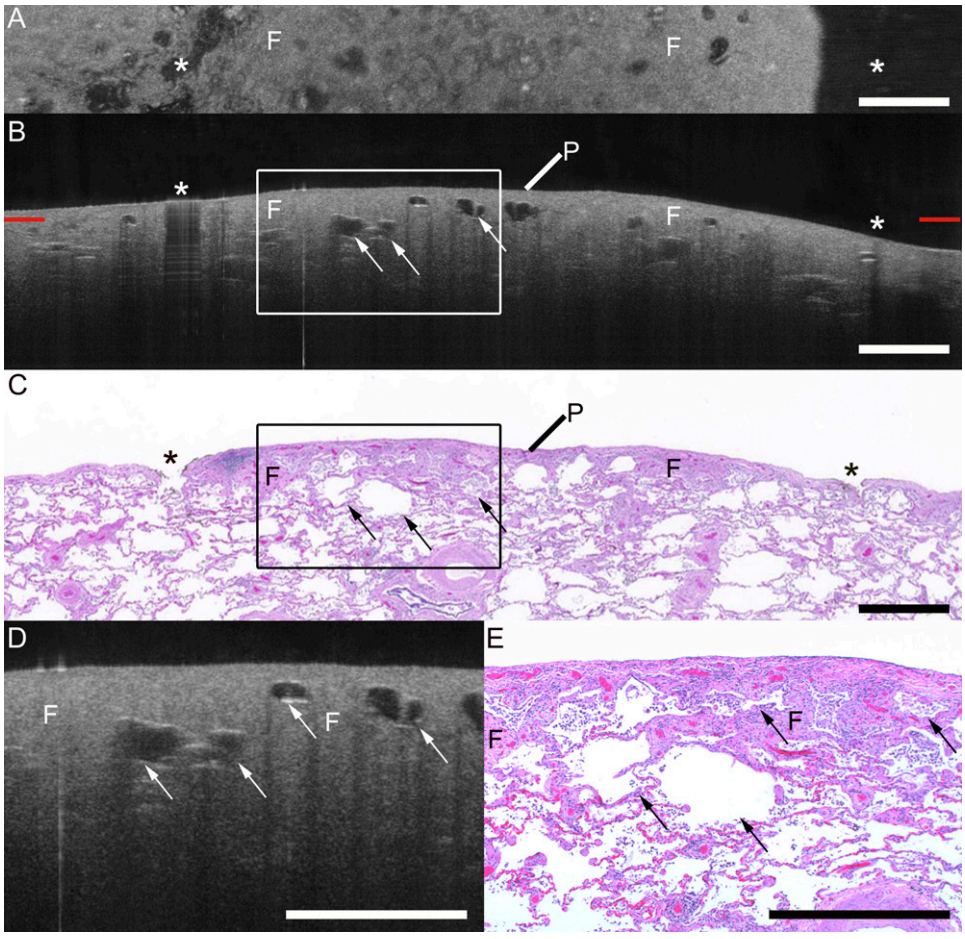

FIGURE 7. Pleural catheter-based OFDI of mild pleural and subpleural interstitial fibrosis. P indicates pleura, and F indicates focal mild pleural fibrosis. A, En face OFDI at location of red side tick marks in B. B and C, OFDI longitudinal section (B) and corresponding histopathology (C) (hematoxylin and eosin stain). D and E, Higher magnification of OFDI longitudinal section (D) and corresponding histopathology at location of boxed region in B and C (D) (hematoxylin and eosin stain). Arrows indicate alveoli, and ink marks are denoted by asterisks. Scale bars = 1.0 mm. See Figure 1 legend for expansion of abbreviation.

which would be useful to increase diagnostic yield in tumors that typically arise in the central airways, such as SCCs and neuroendocrine tumors. OFDI could play a particularly useful role in surveying large volumes of airway to possibly detect early lesions that are not visible bronchoscopically. Parenchymal OFDI would be useful in evaluating peripheral disease, including invasive adenocarcinomas, bronchioloalveolar carcinomas, and benign lesions such as hamartomas, and could potentially be achieved through needle probe-based imaging during CT scan-guided percutaneous procedures. Future studies are aimed at developing transbronchial OFDI catheters, which would be of particular use to confirm correct needle placement prior to transbronchial biopsy when the lesion of interest is small and peripheral. In the present study, parenchymal imaging was primarily performed by imaging peripheral tissue with an OFDI catheter through pleural incisions to act as a proxy to needle probe imaging.

In addition to guiding biopsy site selection, there are numerous other potential clinical applications for pulmonary OFDI. The acquisition of large volumetric OFDI data sets may provide a form of additional virtual tissue to accompany standard biopsy specimens. When biopsy samples are insufficiently sized, the virtual tissue may provide additional architectural information for diagnosis and may potentially minimize the need for additional ancillary tests frequently performed for histologic subtyping.[48-54] Patients may also possibly be spared high-risk invasive surgical procedures if OFDI is capable of differentiating benign from malignant lesions, such as in the cartilaginous hamartoma presented in the current study. In order for OFDI to be used in these types of clinical settings, the imaging features of a variety of pulmonary pathologies would have to be established and validated in a large-scale study, which will be the aim of future studies.

Imaging of ex vivo lung specimens presents some limitations when used as a surrogate for in vivo imaging.

Table 1—*Summary of Optical Frequency Domain Imaging Findings*

Pathology	Imaging Features
Normal	
Airway	Layered architecture, including respiratory epithelium and underlying basement membrane, lamina propria, and cartilaginous rings
Parenchyma	Thin, lattice-like alveolar architecture with signal-void spaces
Neoplastic	
Adenocarcinoma	Loss of layered architecture Mass with signal heterogeneity with rapid attenuation Atypical gland formation
Mucinous adenocarcinoma	Signal-intense alveolar wall thickening Preserved lattice-like architecture Signal-poor intraalveolar mucin Homogeneous signal-intense tumor-associated scar may be seen
Squamous cell carcinoma, basaloid type	Loss of layered architecture Mass with signal heterogeneity and rapid attenuation Irregular tumor nests with signal-intense periphery corresponding to malignant cells and signal-poor center corresponding to central necrosis
Salivary gland adenocarcinoma, adenoid cystic carcinoma	Luminal mass protrusion Uniform distribution of signal-intense trabeculae Small pseudocystic spaces filled with mucin can be seen Intact overlying respiratory epithelium may be present
Benign	
Cartilaginous hamartoma	Lobulated mass with well-delineated borders and evenly dispersed, fine-scale regions of high signal intensity and background of uniform, moderate signal intensity
Fibrosis	
Usual interstitial fibrosis	Diffuse, signal-dense subpleural fibrosis Irregular-shaped, signal-poor subpleural cysts
Focal mild subpleural fibrosis, idiopathic	Focal, signal-dense pleural fibrosis Interspersed lattice-like alveoli with mildly thickened alveolar walls

Resected lung specimens are uninflated and can undergo atelectasis as a surgical artifact. This alters the appearance of the normal alveolar structures and may alter the appearance of smaller airways because of lack of airway traction by attached inflated alveoli. Specifically, the ability to assess airspace enlargement is hindered by the lack of inflation, which will be important in the in vivo setting to distinguish emphysematous change from overinflation, and cystic change associated with fibrosis. However, cystic changes seen in the setting of fibrosis would be accompanied by fibrotic lung parenchyma. In this article, we demonstrate that fibrotic lung parenchyma is visible on OFDI, even in uninflated specimens, and therefore, we do not anticipate any difficulties in differentiating cystic change associated with fibrosis from emphysematous changes and overinflation. Imaging inflated, surgically resected samples with tissue marking for histopathology correlation is technically challenging. Lobectomy and pneumonectomy specimens may be inflated during imaging by attaching the resected bronchus to a pressurized inflation system. However, most surgical lung specimens are received after pathology frozen section evaluation, during which the pathologist must cut the pleural surface and parenchyma to assess the malignancy, hindering the ability to inflate the specimen. Nonpathologic atelectasis is not present in the in vivo setting; thus, this limitation would not extend to in vivo OFDI pulmonary imaging. Future studies will be aimed at developing protocols to image inflated ex vivo specimens to reduce artifactual atelectasis and provide a closer model of in vivo imaging.

Motion artifacts may be present in the in vivo setting where they are not present in ex vivo imaging; however, given that the rapid frame rates of OFDI systems are currently approaching ≥ 200 frames/s (frame size, $512 \times 1{,}024$ pixels),[55-57] it is not anticipated that this will be a significant issue. Previous in vivo OCT and OFDI studies have proven to be successful with the visualization of fine imaging features.[28-33,43,44]

There are some limitations to OCT and OFDI as they apply to pulmonary imaging. OCT and OFDI are currently unable to reliably differentiate smooth muscle from the other tissues of the lamina propria. However, in the context of airway malignancy, the precise identification of smooth muscle is less significant in terms of diagnosis because any invasion into the lamina propria would constitute an invasive malignancy. Identification of early airway malignancies, including in situ lesions, will be addressed in future studies. It can also be difficult to distinguish vascular structures from other signal-void structures if there is no shadow artifact associated with the vascular structure. The addition of Doppler OCT and OFDI to structural OCT and OFDI would aid in the identification of vessels. The cartilage seen in the cartilaginous hamartoma has different OFDI signal properties than the cartilage seen in bronchial cartilage rings. Given the limited number of hamartomas imaged in this study, the cause for the discrepancy cannot be determined but will be addressed in future large-scale studies. Inflammatory lesions, such as granulomatous lesions, have not been included in this study because these types of lesions are not frequently resected. However,

future large-scale studies will need to include inflammatory lesions to determine whether they can be differentiated from malignant lesions. Finally, discriminating tumor from tumor-associated scar could also prove to be problematic in some cases, and this will be further evaluated in future studies with larger numbers of specimens.

In this study, we provide initial image feature interpretations of common benign and malignant lung lesions and interstitial fibrosis by accurately correlating OFDI with histopathology. We demonstrate that OFDI can be precisely correlated with histopathology with the use of simple ink-marking techniques visible in both imaging and histology. Both bronchoscopic and parenchymal ex vivo OFDI is assessed with correlated histology to evaluate imaging features of common pulmonary pathology, which can be applied to in vivo imaging. However, before OFDI can take on a more useful role in interpreting pulmonary disease in vivo, a more extensive investigation must be performed to determine specifically what pathologic entities and features are evaluable with OFDI. This requires a large-scale OFDI study of pulmonary specimens, with one-to-one matched OFDI to histopathology, evaluating a variety of pulmonary pathologies. Such future studies will be performed for the development and validation of imaging criteria through blinded expert assessment of datasets to determine imaging criteria sensitivity and specificity as well as interobserver agreement.

Acknowledgments

Author contributions: Dr Suter had full access to all of the data in the study and takes responsibility for the integrity of the data and the accuracy of the data analysis.
Dr Hariri: contributed to the study design; collection, analysis, and interpretation of data; drafting and critical review of the manuscript; and reading and approval of the final version of the manuscript.
Mr Applegate: contributed to the collection and analysis of data, critical review of the manuscript, and reading and approval of the final version of the manuscript.
Dr Mino-Kenudson: contributed to the collection, analysis, and interpretation of data; critical review of the manuscript; and reading and approval of the final version of the manuscript.
Dr Mark: contributed to the collection, analysis, and interpretation of data; critical review of the manuscript; and reading and approval of the final version of the manuscript.
Dr. Medoff: contributed to the collection of data, critical review of the manuscript, and reading and approval of the final version of the manuscript.
Dr Luster: contributed to the collection of data, critical review of the manuscript, and reading and approval of the final version of the manuscript.
Dr Bouma: contributed to the development of the imaging technology and catheters, critical review of the manuscript, and reading and approval of the final version of the manuscript.
Dr. Tearney: contributed to the development of the imaging system, analysis and interpretation of data, critical review of the manuscript, and reading and approval of the final version of the manuscript.
Dr Suter: contributed to the study design; development of the imaging system and catheters; collection, analysis, and interpretation of data; drafting and critical review of the manuscript; and reading and approval of the final version of the manuscript.
Financial/nonfinancial disclosures: The authors have reported to *CHEST* the following conflicts of interest: Drs Bouma and Tearney receive consulting income from NinePoint Medical, Inc. Dr Suter receives clinical research support from NinePoint Medical, Inc. NinePoint Medical, Inc has a licensing arrangement with Massachusetts General Hospital. Drs Tearney, Bouma, and Suter have the right to receive royalty payments from NinePoint Medical, Inc. Drs Hariri, Mino-Kenudson, Mark, Medoff, and Luster and Mr Applegate have reported that no potential conflicts of interest exist with any companies/organizations whose products or services may be discussed in this article.
Role of sponsors: The sponsors had no role in the design of the study, the collection and analysis of the data, or in the preparation of the manuscript.
Other contributions: We thank Sven Holder, BS; Stephen Conley; Milen Shishkov, PhD; Kevin Gallagher, BS; and the Wellman Center for Photomedicine Photopathology core for their contributions to this work.
Additional information: The Video can be found in the "Supplemental Materials" area of the online article.

References

1. Jemal A, Siegel R, Ward E, Murray T, Xu J, Thun MJ. Cancer statistics, 2007. *CA Cancer J Clin*. 2007;57(1):43-66.
2. Huang D, Swanson EA, Lin CP, et al. Optical coherence tomography. *Science*. 1991;254(5035):1178-1181.
3. Bouma BE, Tearney GJ, Compton CC, Nishioka NS. High-resolution imaging of the human esophagus and stomach in vivo using optical coherence tomography. *Gastrointest Endosc*. 2000;51(4):467-474.
4. Yun S, Tearney G, de Boer J, Iftimia N, Bouma B. High-speed optical frequency-domain imaging. *Opt Express*. 2003;11(22): 2953-2963.
5. Yun SH, Tearney GJ, Vakoc BJ, et al. Comprehensive volumetric optical microscopy in vivo. *Nat Med*. 2006;12(12): 1429-1433.
6. Yun S, Tearney G, Bouma B, Park B, de Boer J. High-speed spectral-domain optical coherence tomography at 1.3 mum wavelength. *Opt Express*. 2003;11(26):3598-3604.
7. Yun S, Tearney G, de Boer J, Bouma B. Removing the depth-degeneracy in optical frequency domain imaging with frequency shifting. *Opt Express*. 2004;12(20):4822-4828.
8. Choma M, Sarunic M, Yang C, Izatt J. Sensitivity advantage of swept source and Fourier domain optical coherence tomography. *Opt Express*. 2003;11(18):2183-2189.
9. Brezinski ME, Tearney GJ, Bouma BE, et al. Optical coherence tomography for optical biopsy. Properties and demonstration of vascular pathology. *Circulation*. 1996;93(6): 1206-1213.
10. Tearney GJ, Waxman S, Shishkov M, et al. Three-dimensional coronary artery microscopy by intracoronary optical frequency domain imaging. *JACC Cardiovasc Imaging*. 2008; 1(6):752-761.
11. Fujimoto JG, Boppart SA, Tearney GJ, Bouma BE, Pitris C, Brezinski ME. High resolution in vivo intra-arterial imaging with optical coherence tomography. *Heart*. 1999;82(2): 128-133.
12. Bezerra HG, Costa MA, Guagliumi G, Rollins AM, Simon DI. Intracoronary optical coherence tomography: a comprehensive review clinical and research applications. *JACC Cardiovasc Interv*. 2009;2(11):1035-1046.
13. Farooq V, Serruys PW, Heo JH, et al. New insights into the coronary artery bifurcation hypothesis-generating concepts utilizing 3-dimensional optical frequency domain imaging. *JACC Cardiovasc Interv*. 2011;4(8):921-931.

14. Gogas BD, Farooq V, Onuma Y, et al. 3-dimensional optical frequency domain imaging for the evaluation of primary percutaneous coronary intervention in ST-segment elevation myocardial infarction. *Int J Cardiol*. 2011;151(1):103-105.
15. Kubo T, Xu C, Wang Z, van Ditzhuijzen NS, Bezerra HG. Plaque and thrombus evaluation by optical coherence tomography. *Int J Cardiovasc Imaging*. 2011;27(2):289-298.
16. Prati F, Jenkins MW, Di Giorgio A, Rollins AM. Intracoronary optical coherence tomography, basic theory and image acquisition techniques. *Int J Cardiovasc Imaging*. 2011;27(2): 251-258.
17. Prati F, Regar E, Mintz GS, et al; Expert's OCT Review Document. Expert review document on methodology, terminology, and clinical applications of optical coherence tomography: physical principles, methodology of image acquisition, and clinical application for assessment of coronary arteries and atherosclerosis. *Eur Heart J*. 2010;31(4):401-415.
18. Tearney GJ, Brezinski ME, Bouma BE, et al. In vivo endoscopic optical biopsy with optical coherence tomography. *Science*. 1997;276(5321):2037-2039.
19. Suter MJ, Vakoc BJ, Yachimski PS, et al. Comprehensive microscopy of the esophagus in human patients with optical frequency domain imaging. *Gastrointest Endosc*. 2008;68(4): 745-753.
20. Aguirre AD, Chen Y, Bryan B, et al. Cellular resolution ex vivo imaging of gastrointestinal tissues with optical coherence microscopy. *J Biomed Opt*. 2010;15(1):016025.
21. Chen Y, Aguirre AD, Hsiung PL, et al. Ultrahigh resolution optical coherence tomography of Barrett's esophagus: preliminary descriptive clinical study correlating images with histology. *Endoscopy*. 2007;39(7):599-605.
22. Qi X, Pan Y, Sivak MV, Willis JE, Isenberg G, Rollins AM. Image analysis for classification of dysplasia in Barrett's esophagus using endoscopic optical coherence tomography. *Biomed Opt Express*. 2010;1(3):825-847.
23. Testoni PA, Mangiavillano B. Optical coherence tomography in detection of dysplasia and cancer of the gastrointestinal tract and bilio-pancreatic ductal system. *World J Gastroenterol*. 2008;14(42):6444-6452.
24. Yang Y, Whiteman S, Gey van Pittius D, He Y, Wang RK, Spiteri MA. Use of optical coherence tomography in delineating airways microstructure: comparison of OCT images to histopathological sections. *Phys Med Biol*. 2004;49(7): 1247-1255.
25. Hanna N, Saltzman D, Mukai D, et al. Two-dimensional and 3-dimensional optical coherence tomographic imaging of the airway, lung, and pleura. *J Thorac Cardiovasc Surg*. 2005;129(3):615-622.
26. Xie T, Liu G, Kreuter K, et al. In vivo three-dimensional imaging of normal tissue and tumors in the rabbit pleural cavity using endoscopic swept source optical coherence tomography with thoracoscopic guidance. *J Biomed Opt*. 2009; 14(6):064045.
27. Quirk BC, McLaughlin RA, Curatolo A, Kirk RW, Noble PB, Sampson DD. In situ imaging of lung alveoli with an optical coherence tomography needle probe. *J Biomed Opt*. 2011; 16(3):036009.
28. Coxson HO, Lam S. Quantitative assessment of the airway wall using computed tomography and optical coherence tomography. *Proc Am Thorac Soc*. 2009;6(5):439-443.
29. Coxson HO, Quiney B, Sin DD, et al. Airway wall thickness assessed using computed tomography and optical coherence tomography. *Am J Respir Crit Care Med*. 2008;177(11): 1201-1206.
30. Lam S, Standish B, Baldwin C, et al. In vivo optical coherence tomography imaging of preinvasive bronchial lesions. *Clin Cancer Res*. 2008;14(7):2006-2011.
31. Michel RG, Kinasewitz GT, Fung KM, Keddissi JI. Optical coherence tomography as an adjunct to flexible bronchoscopy in the diagnosis of lung cancer: a pilot study. *Chest*. 2010; 138(4):984-988.
32. Tsuboi M, Hayashi A, Ikeda N, et al. Optical coherence tomography in the diagnosis of bronchial lesions. *Lung Cancer*. 2005;49(3):387-394.
33. Whiteman SC, Yang Y, Gey van Pittius D, Stephens M, Parmer J, Spiteri MA. Optical coherence tomography: real-time imaging of bronchial airways microstructure and detection of inflammatory/neoplastic morphologic changes. *Clin Cancer Res*. 2006;12(3 pt 1):813-818.
34. Armstrong J, Leigh M, Walton I, et al. In vivo size and shape measurement of the human upper airway using endoscopic longrange optical coherence tomography. *Opt Express*. 2003; 11(15):1817-1826.
35. Armstrong JJ, Leigh MS, Sampson DD, Walsh JH, Hillman DR, Eastwood PR. Quantitative upper airway imaging with anatomic optical coherence tomography. *Am J Respir Crit Care Med*. 2006;173(2):226-233.
36. McLaughlin RA, Armstrong JJ, Becker S, et al. Respiratory gating of anatomical optical coherence tomography images of the human airway. *Opt Express*. 2009;17(8):6568-6577.
37. McLaughlin RA, Williamson JP, Phillips MJ, et al. Applying anatomical optical coherence tomography to quantitative 3D imaging of the lower airway. *Opt Express*. 2008;16(22): 17521-17529.
38. Noble PB, McLaughlin RA, West AR, et al. Distribution of airway narrowing responses across generations and at branching points, assessed in vitro by anatomical optical coherence tomography. *Respir Res*. 2010;11:9.
39. Noble PB, West AR, McLaughlin RA, et al. Airway narrowing assessed by anatomical optical coherence tomography in vitro: dynamic airway wall morphology and function. *J Appl Physiol*. 2010;108(2):401-411.
40. Williamson JP, Armstrong JJ, McLaughlin RA, et al. Measuring airway dimensions during bronchoscopy using anatomical optical coherence tomography. *Eur Respir J*. 2010;35(1):34-41.
41. Williamson JP, McLaughlin RA, Phillips MJ, et al. Using optical coherence tomography to improve diagnostic and therapeutic bronchoscopy. *Chest*. 2009;136(1):272-276.
42. Delacretaz Y, Shaffer E, Pavillon N, Kuhn J, Lang F, Depeursinge C. Endoscopic low-coherence topography measurement for upper airways and hollow samples. *J Biomed Opt*. 2010;15(6):066014.
43. Su J, Zhang J, Yu L, G Colt H, Brenner M, Chen Z. Real-time swept source optical coherence tomography imaging of the human airway using a microelectromechanical system endoscope and digital signal processor. *J Biomed Opt*. 2008;13(3): 030506.
44. Suter MJ, Riker DR, Gallagher KA, et al. Real-time comprehensive microscopy of the pulmonary airways: a pilot clinical study [Abstract]. *Am J Respir Crit Care Med*. 2010;181:A5159.
45. Hariri LP, Applegate MB, Mino-Kenudson M, et al. Optical frequency domain imaging of ex vivo pulmonary resection specimens. Obtaining one to one image to histopathology correlation. *J Vis Exp*. In press.
46. Sakamoto A, Hangai M, Yoshimura N. Spectral-domain optical coherence tomography with multiple B-scan averaging for enhanced imaging of retinal diseases. *Ophthalmology*. 2008;115(6):1071-1078.
47. McLean M, Prothero JW. Three-dimensional reconstruction from serial sections. V. Calibration of dimensional changes incurred during tissue preparation and data processing. *Anal Quant Cytol Histol*. 1991;13(4):269-278.
48. Cooper WA, O'Toole S, Boyer M, Horvath L, Mahar A. What's new in non-small cell lung cancer for pathologists:

the importance of accurate subtyping, EGFR mutations and ALK rearrangements. *Pathology*. 2011;43(2):103-115.
49. Loo PS, Thomas SC, Nicolson MC, Fyfe MN, Kerr KM. Subtyping of undifferentiated non-small cell carcinomas in bronchial biopsy specimens. *J Thorac Oncol*. 2010;5(4): 442-447.
50. Mukhopadhyay S, Katzenstein AL. Subclassification of non-small cell lung carcinomas lacking morphologic differentiation on biopsy specimens: utility of an immunohistochemical panel containing TTF-1, napsin A, p63, and CK5/6. *Am J Surg Pathol*. 2011;35(1):15-25.
51. Nicholson AG, Gonzalez D, Shah P, et al. Refining the diagnosis and EGFR status of non-small cell lung carcinoma in biopsy and cytologic material, using a panel of mucin staining, TTF-1, cytokeratin 5/6, and P63, and EGFR mutation analysis. *J Thorac Oncol*. 2010;5(4):436-441.
52. Pelosi G, Rossi G, Bianchi F, et al. Immunhistochemistry by means of widely agreed-upon markers (cytokeratins 5/6 and 7, p63, thyroid transcription factor-1, and vimentin) on small biopsies of non-small cell lung cancer effectively parallels the corresponding profiling and eventual diagnoses on surgical specimens. *J Thorac Oncol*. 2011;6(6):1039-1049.
53. Rekhtman N, Ang DC, Sima CS, Travis WD, Moreira AL. Immunohistochemical algorithm for differentiation of lung adenocarcinoma and squamous cell carcinoma based on large series of whole-tissue sections with validation in small specimens. *Mod Pathol*. 2011;24(10):1348-1359.
54. Righi L, Graziano P, Fornari A, et al. Immunohistochemical subtyping of nonsmall cell lung cancer not otherwise specified in fine-needle aspiration cytology: a retrospective study of 103 cases with surgical correlation. *Cancer*. 2011;117(15): 3416-3423.
55. Braaf B, Vermeer KA, Sicam VA, van Zeeburg E, van Meurs JC, de Boer JF. Phase-stabilized optical frequency domain imaging at 1-μm for the measurement of blood flow in the human choroid. *Opt Express*. 2011;19(21):20886-20903.
56. Oh WY, Vakoc BJ, Shishkov M, Tearney GJ, Bouma BE. >400 kHz repetition rate wavelength-swept laser and application to high-speed optical frequency domain imaging. *Opt Lett*. 2010;35(17):2919-2921.
57. Gora M, Karnowski K, Szkulmowski M, et al. Ultra high-speed swept source OCT imaging of the anterior segment of human eye at 200 kHz with adjustable imaging range. *Opt Express*. 2009;17(17):14880-14894.